Final Draft
of the original manuscript:

Application of scanning electrode techniques for the evaluation of iron-zinc corrosion in nearly neutral chloride solutions

A.G. Marques[1], M. Taryba[1], A. S. Panão[1], S. Lamaka[1,a], A.M. Simões[1*]

[1]*CQE – Centro de Química Estrutural and Department of Chemical Engineering, Instituto Superior Técnico, Universidade de Lisboa, Av. Rovisco Pais, 1049-001 Lisboa, Portugal*

* Corresponding author: alda.simoes@tecnico.ulisboa.pt

[a] *Present address: MagIC - Magnesium Innovation Centre, Institute of Materials Research, Helmholtz-Zentrum, Geesthacht, 21502, Germany*

Abstract

A model electrode consisting of a narrow zinc anode and a split iron cathode was used for assessing galvanic corrosion at cut edges. This setup aimed at a better understanding of the mechanisms of galvanic corrosion at cut edges and of the effective resolution of microprobe electrochemical techniques, namely the scanning electrochemical microscope (SECM), the localized electrochemical impedance spectroscopy (LEIS) and the scanning vibrating electrode technique coupled with the scanning ion-selective electrode technique (SVET/SIET).

Hydroxyl ions diffuse across the cathode, in the direction of the anode, until they reach the critical area of precipitation above the cathode, at a distance from the edge of the cathode. The zinc corrosion products ultimately precipitate on the iron cathode, once the critical pH and solubility limits for precipitation of zinc corrosion is reached, at a distance from the edge that is determined by the diffusion of Zn^{2+} and counter-diffusion of OH^-. These precipitates revealed no inhibition on the cathodic reaction.
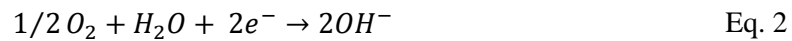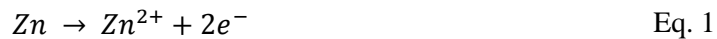
The local activity on the zinc was easily detected by the LEIS and the SVET, whereas the zinc corrosion products were detected by the SECM. The local a.c. admittance measured on the cathode closer to the zinc anode at the early stages was insensitive to the local activity despite the d.c. ionic current measured in solution, whereas for longer immersion times an increase of admittance is explained by an increase in the solution conductivity.

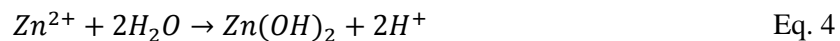**Keywords:** galvanic corrosion; LEIS; SECM; SVET; SIET

1. Introduction

Electrogalvanized steel strip is a cost effective and versatile solution to produce automobile body parts. The application of just a few micrometers of zinc results in a light-weighed, weldable and corrosion resistant structural material, especially if coil-coated with an organic layer. In this technology, vulnerability of cut edges is a matter of great concern to manufacturers due to the formation of a galvanic couple with a high electromotive force and an unfavourable anode-to-cathode area ratio. On steel, where oxygen reduction proceeds under diffusion control, a great demand of electrons is satisfied by the oxidation of zinc, which will corrode at a high rate eventually leading to coil-coating delamination and consequent failure of the material.

In aqueous environments of neutral pH, zinc dissolves into the solution; whereas oxygen reduction on steel is the main cathodic reaction and leads to alkalinisation of the electrolyte near the cathode:
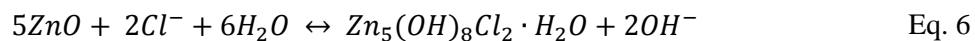
$$Zn \rightarrow Zn^{2+} + 2e^- \qquad\qquad \text{Eq. 1}$$

$$1/2\,O_2 + H_2O + 2e^- \rightarrow 2OH^- \qquad\qquad \text{Eq. 2}$$

The dissolved Zn^{2+} may react with H_2O, producing either zincyl ion ($ZnOH^+$), Eq. 3, or zinc hydroxide, $Zn(OH)_2$, Eq. 4, depending on the pH,:

$$Zn^{2+} + H_2O \rightarrow ZnOH^+ + H^+ \qquad\qquad \text{Eq. 3}$$

$$Zn^{2+} + 2H_2O \rightarrow Zn(OH)_2 + 2H^+ \qquad\qquad \text{Eq. 4}$$

Zinc oxide (ZnO) can also be formed directly from zinc hydroxide by dehydration:

$$Zn(OH)_2 \rightarrow ZnO + H_2O \qquad\qquad \text{Eq. 5}$$

Briefly, the mechanism of cut edge corrosion and precipitation of zinc compounds can be described by the formation of $ZnOH^+$ at pH <7-9 and precipitation of $Zn(OH)_2$ and ZnO by reduction of oxygen at more alkaline solutions. In concentrated chloride solutions, simonkolleite ($Zn_5(OH)_8Cl_2 \cdot 2H_2O$) can also be formed according to Eq. 6.

$$5ZnO + 2Cl^- + 6H_2O \leftrightarrow Zn_5(OH)_8Cl_2 \cdot H_2O + 2OH^- \qquad\qquad \text{Eq. 6}$$

At pH 9-11 zinc cations become insoluble and precipitation of zinc neutral species occurs above the steel [1]. The alkalinisation near the steel surface has been confirmed by Thébault et al. [3], who found values between 9-10 at the center of the steel plate and a nearly constant pH ~8 above the corrosion products, whereas a nearly neutral pH was registered above

zinc. Further, mapping of the ionic current density has lead to the identification of a region of hindered cathodic activity on the steel of a cut edge, located on a region closer to the zinc anode, in which there was approximate absence of ionic current [3], on which a thin insulating film has been considered. The transport of charged species is thus essential; according to Tada et al. [6, 7, 8], zinc cations remain confined to a 1 mm layer of solution above zinc and part of the steel, corresponding to the lowest pH regions, whereas far away from the anode, at the highest pH regions, almost no free Zn^{2+} was reported. Finally, in the boundary region, a layer of zinc corrosion products was formed, meaning that all zinc cations in solution formed insoluble species.

The nature of the white zinc corrosion products has also been discussed in the literature. Bonk et al. [9] identified both ZnO and $Zn(OH)_2$, under neutral pH and suggested that for increasing pH values, anions present in solution diffuse into this layer and react with the cations to form zinc complexes, resulting in a more porous layer with a $Zn(OH)_2$ matrix. Contaminants like carbon dioxide favour the formation of hydrozincite ($Zn_5(CO_3)_2(OH)_6$), whereas chloride favours the formation of simonkolleite [10]. Padilla et al. [11] and Krieg et al. [12], in line with previous work from Tanaka et al. [13], stated that in addition to zinc corrosion products, interaction of Zn^{2+} with iron oxides may cause inhibition of the cathodic reaction by suppressing the crystallization and growth of $\beta - FeOOH$. In recent publications, Ogle et al [14, 15, 16] reported inhibition of the cathodic reaction on iron in the presence of synthetic simonkolleite, which was lost at very alkaline pH when this species became converted to either hydrozincite or zinc oxide; species like hydrozincite, sodium zinc carbonate and zinc hydroxyl sulfate revealed lower cathodic inhibition than simonkolleite. Mouanga et al. [17, 18] have concluded that corrosion products in NaCl and NaOH solutions do not suppress cathodic reaction on zinc and instead supported the theory of a synergistic effect of iron and zinc cations as proposed by Tanaka et al. [13].

The understanding of cut edge corrosion has gained momentum with the development of electrochemical microprobe techniques. These techniques provide enhanced lateral resolution and consequently the possibility of measuring small variations in the electric fields and local distribution of ionic currents as revealed by the pioneer work from Isaacs et al. [19] and applied by Worsley et al. [20], Zou et al. [21] and Thébault et al. [4] to the study of cut edge corrosion. Thus, mapping of pH using a tungsten solid electrode over cut edges and model systems has revealed a strong pH gradient over the cathode [3, 6, 22]. The pH and zinc concentration gradients have been further studied by the use of scanning electrochemical microscopy with antimony and mercury microelectrodes by Souto et al. [22, 23, 24] and with an ion selective micro-electrode (ISME) by Terryn et al. [25]. In previous studies from our own group, the ionic

current distribution was studied using the SVET [26] and the SECM [27] and cathodic inhibition was found due to the presence of zinc corrosion products; nevertheless, limitations of the SECM due to precipitation of zinc corrosion products on the microprobe surface was reported. More recently, mapping of the conductivity of a cut edge by the feedback current corresponding to oxidation of a redox mediator in SECM measurements, suggested reciprocal a correlation with the distribution of zinc corrosion products [28]. Localized electrochemical impedance spectroscopy has also been applied to the study of galvanic systems. Mouanga et al. [29] used a disk-type concentric zinc-steel electrode and concluded that the local ohmic impedance was highly affected by the radial position of the probe, whereas a local current maximum was observed at the zinc/steel interface, indicating a highly localized corrosion process. Despite the enhanced spatial resolution of these techniques, the actual lateral resolution when it comes to cut edge corrosion is hard to establish, because of the small electrode size and of the direct contact between anode and cathode, which results in large gradients of current, potential and pH. Attempts to overcome this limitation have been made using numerical modelling to simulate current [4, 30] and pH distributions [31], but an alternative to overcome the resolution problem is to perform studies on model systems with enlarged dimensions and physically separate anodes and cathodes, such that ions spread over a larger area, making the concentration, current and pH gradients smoother and more easily detected by the microprobes. Bearing this in mind, we have designed a model for a single side coated cut edge, in which zinc is separated from iron by a thick resin layer; further, the iron is split in two halves, located on the same side of the anode. With this asymmetric geometry, we expect to prevent any influence of the signal from zinc on the measurements made over iron, allowing an improved resolution of cathode and anode. The discontinuity of the cathodes should allow for a better separation of the response from the regions covered and uncovered by zinc corrosion products. In this way we expected to monitor individual process occurring at each of the metal plates without the interference of the reactions occurring on the neighbour material.

2. Experimental

2.1 Electrodes and electrolytes

Samples cut from an iron plate with 1 mm thickness and a 50 μm zinc foil, both with purity 99.95% (Goodfellow, Cambridge, U.K) were employed as electrodes for building the model for galvanic corrosion. The model consisted of one zinc electrode and two iron electrodes, mounted on an epoxy resin sleeve with their edges parallel to each other - Figure 1. The working surface of the mount was grounded with silicon carbide paper under ethanol until 1000 grit finish, then rinsed in ethanol and dried under blown cold air. The last polishing step

was made along the direction of the iron-zinc interface to minimize spreading of zinc onto the iron surface. Electrical connection between the metals was assured through an external circuit in the rear of the mount consisting of copper wires connected to the foils with conductive silver paint (SPI® Supplies, USA). A small electrochemical cell was built by surrounding the epoxy sleeve with adhesive tape and filling it with ca. 3.5 mL of electrolyte. All experiments were carried out in a quiescent 10 mM NaCl electrolyte with conductivity $k = 1088\,\mu S$ at 22.5 ºC. The pH and conductivity of the solutions were measured using a bench top multi-parameter Eutech PC 700 (Eutech Instruments, Singapore). Deionized water (MilliPore, $\rho > 18$ MΩ cm) and analytical grade chemicals from Sigma-Aldrich were employed.

2.2 Corrosion monitoring

2.2.1 Potential-time DC curves

DC potential-time curves at open circuit were made using an ACM Field Machine (ACM Instruments, U.K.) and ACM software v5. A KCl-saturated calomel electrode (SCE) was used as reference electrode. *In-situ* image recording of the corroding model was performed using a DMS300 digital microscope system (Leica Microsystems, Switzerland).

2.2.2 Scanning electrochemical microscopy (SECM)

A Uniscan electrochemical interface connected to a M370 workstation (Uniscan Instruments, U.K.) and equipped with a piezoelectric motor positioning system was used for characterization of surface conductivity and oxygen depletion in the vicinity of the model. The system operated in a three-electrode configuration, with the galvanic couple at its free corroding potential in the test solution. The SECM probe (the working electrode) consisted of a platinum disk of 10 μm diameter sheathed in a conical glass rod and the cell was completed with a platinum mesh counter electrode and the SCE as reference. The experiments were performed at room temperature and under natural aeration in a 0.5 mM ferrocenemethanol (abbreviated as FcMeOH, supplied by Sigma-Aldrich, 97%) and 10 mM NaCl (99%) solution. The operating height was set after recording *z*-approach curves with the tip approaching the surface until the current dropped to 30% of the limiting current value; subsequently, the tip was withdrawn to a level estimated as ~20 μm away from the surface. Although the ideal working distance should be in the range of the tip diameter, by proceeding in this way the sample was still kept inside the diffusion layer of the probe, while bumping against corrosion products on the surface was prevented. Linear scans were made at constant height and at a scan rate of 0.5 μm s⁻¹.

Feedback mode: this operating mode was used for the identification of the conductive regions and topographic features on the surface of the model system. It is based upon the variations of the diffusion limiting current at the tip due to reactions involving a redox mediator brought into the vicinity of an electroactive surface. The limiting current at the tip will increase if the (conductive) sample surface is able to regenerate the mediator or decrease if the (insulating) surface cannot regenerate the mediator [32]. The ferrocene / ferrocenium (FcMeOH/ FcMeOH$^+$) was the mediator chosen for this work as it is a well-known fast redox system, whose reversible potential is + 0.216V, well above the free corroding potential of the cut edge and has been applied as mediator in the work of Wipf and Bard [33]. The voltammetric curve of the ultra-microelectrode (UME) in the working solution - Figure 2 (a) - gave a typical sigmoid shape for the oxidation of FcMeOH to FcMeOH$^+$ and the tip potential E= +0.40 V in the diffusion plateau, was chosen for the amperometric studies .

Competition mode: in this mode the tip and the sample compete for the reduction of oxygen within the diffusion layer of the cathode. Of the species available in solution (Na$^+$, Cl$^-$, O$_2$, H$_2$O, H$^+$, Zn^{2+} and FcMeOH), only molecular oxygen and water can be expected to become reduced at moderate polarizations, but reduction of H$_2$O occurs at higher cathodic polarizations. Therefore, based upon the voltammogram in Figure 2 (b), a potential of -0.50 V was chosen for the amperometric measurements.

2.2.3 Localized electrochemical impedance (LEIS) measurements

LEIS was performed with a M370 electrochemical workstation (Uniscan Instruments, UK) coupled to a 1286 potentiostat and a 1250 frequency response analyzer (both by Solartron Analytical, UK). For full spectrum analysis, the applied potential amplitude was 10 mV and frequencies ranged from 10 kHz to 1 Hz, at seven points per decade. The commercial bi-probe (Uniscan Instruments, Cheshire, UK) made with platinum consisted of a 10 µm diameter disk embedded at the bottom of a conical insulating holder and a ring at a distance of 1.5 mm. With this geometry, the probe measures the ionic currents along a direction which is ~30º normal to the sample. A platinum mesh reference electrode, a saturated calomel reference electrode (SCE) and the galvanic model completed the cell. Local impedance is determined as the ratio between the amplitude of the excitation potential applied to the sample (ΔV) and the local a.c. current (i_{loc}). The local current is computed from the a.c. voltage measured on the bi-probe ($\Delta \tilde{V}$), the electrolyte conductivity (k) and the separation between the two electrodes of the bi-probe (d), Eq. 7.

$$Z_{loc} = \frac{\Delta V}{i_{loc}} = \frac{d}{k}\frac{\Delta V}{\Delta \tilde{V}}$$

<div align="right">Eq. 7</div>

Local impedance spectra were measured with the tip positioned at the center of each electrode, whereas single-frequency scans (at 1 Hz) were performed by moving the bi-probe by steps of 127 μm across the electrodes. The time taken for each line scan was c.a. 15 minutes.

2.2.4 *Scanning Vibrating Electrode Technique (SVET) and Scanning Ion-selective Electrode Technique (SIET)*

Commercial equipment manufactured by Applicable Electronics and controlled by ASET software was used to perform both the SVET and the SIET measurements. A dual head stage manipulator (Biomedizinische Geräte, Germany) was mounted on the 3D stepper system motors and used for precise positioning a vibrating probe and a pH sensing microelectrode (pH-SME). The VP was an insulated Pt–Ir microelectrode (MicroProbes, U.S.) with a 16 ± 2 μm diameter Pt-black sphere deposited on the exposed metal tip. The probe vibrated in the vertical (z) and horizontal (x) planes relative to the cell surface, at 124 Hz (z) and 325 Hz (x) and 34 μm amplitude.

The pH was measured using ion-selective microelectrodes (ISMEs) made of a silanized glass-capillary with a tip orifice diameter of 1.8 ± 0.2 μm, filled with a selective ionophore-based oil-like membrane and back-filled with an inner reference solution. Hydrogen Ionophore I-Cocktail B (Ref. 95297) of *Selectrophore* grade (from Fluka) was used as a liquid pH-membrane. The column length of the membrane was about $60-70$ μm. . The pH-SMEs were calibrated using commercial pH buffers of pH 5, 7 and 9, to which the adequate background concentration of NaCl was added, and a Nernstian slope of -58.0 ± 0.6 mV/pH was observed. The vibrating probe and pH-SME were positioned at a fixed height of 50 and 100 μm above the surface. The distance between the probes was kept as 50 ± 5 μm and 30 ± 5 μm in the vertical plane and the horizontal plane, respectively [34]. The aqueous solutions were prepared with salts of the highest purity available using de-ionized water (MilliPore, $\rho > 18$ MOhm cm) and all measurements were performed in a 0.01 M NaCl pH neutral solution, using an Ag/AgCl reference mini-electrode with agar-stabilized 0.05 M NaCl salt bridge. The cell was kept in a Faraday cage at ambient temperature (26 ± 2 °C). Line scans having 7545 μm with 49 μm step were obtained in *quasi-simultaneous fashion*, i.e. for each point in the scan grid, current and pH data were obtained sequentially with the time lag of 2.2 seconds. The time required for each scan was 12 minutes.

3. Results

Corrosion of the galvanic couple occurred with precipitation of white corrosion products over iron. This precipitate was dense along a well-defined line and became diffuse, with a lower coverage and an apparently rougher morphology, away from the anode. The precipitate became visible in the first 30 minutes of immersion and was concentrated along a thin wavy line on the center of the inner cathode - Fig. 3 (a-c) whereas the outer cathode (Fe2) remained clean of corrosion products for most of the duration of the experiment. The precipitate consists of zinc oxide or hydroxides (Fig. 3d), can be explained by the diffusion of zinc cations across the galvanic cell and by their subsequent precipitation over the cathode, where the electrolyte becomes alkaline as a result of the reduction of dissolved oxygen according to Eq.(2). The location of the precipitates was however surprising, as they were not visible at the edge, where the cathodic current should be maximum (due to a lower electrolyte resistance) but rather at some distance from the edge. This distribution is very similar to what has been observed on cut edges in our previous work [28] and also in the work from Thébault et al. [4] despite the wide insulating surface separating the cathode and the anode. For zinc ions to remain soluble, the pH at the edge must therefore remain below the critical value given by the solubility product of $Zn(OH)_2$, which is $K_{sp} = 2.66x10^{-15}$ [35], i.e., precipitation cannot occur at pH < 9.71 [36], even at trace concentration of zinc, $\sim 10^{-5}$ M.

The free corrosion potential of the galvanic couple - Figure 4- went through a minimum as the native oxides became dissolved and afterwards took a fairly steady value with some fluctuations, resulting probably from the establishment of concentration gradients and formation of corrosion products. The total variation in the first seven hours was below 20 mV and after 24 hours the potential was relatively stable at around -1.01 V, which is typical of zinc dissolution occurring under oxygen diffusion control [16, 37].

3.1. Local Electrochemical Impedance Spectroscopy, LEIS

The local impedance spectra measured over each of the three electrodes show in some cases an inductive loop at the high frequencies, Figure 5. This loop was observed clearly on the zinc electrode and also on the remote cathode, but not in the inner iron electrode, possibly because of a smaller geometrical distortion of the ionic flow [29]. The high and medium frequency portion of the spectrum is resistive, whereas at frequencies below ~100 Hz a constant-phase-element slope is observed, which corresponds to 10^{-4} $Fcm^{-2}s^{n-1}$ (with n=0.85) for both Fe1 and Fe2 and 10^{-3} $Fcm^{-2}s^{n-1}$ (with n=0.89) on zinc. Comparable values have been

reported for the zinc dissolution process [38]. In this frequency range, a charge transfer resistance of 10^2 Ωcm^2 can be extracted from fitting of the spectrum over zinc, but not on the iron cathodes. A fixed frequency of 1 Hz was chosen to perform linear scans, as the low frequency range is associated with the corrosion processes. The admittance profiles reveal well defined maximum on zinc and on the remote cathode, while on the inner cathode the admittance started at very low values and consistently increased with time - Figure 6. This trend was surprising and is opposite to what is expected from the progressive precipitation of corrosion products on the inner cathode observed in Figure 3.

3.3 Amperometric measurements with the SECM

The current at the tip showed a significant drift which was time related, such that the local currents near the surface easily became smaller than the limiting current (measured immediately before each scan), resulting in an apparent negative feedback across the entire sample. The z-approach curves (not shown) revealed a baseline that effectively corresponds to negative feedback above the resin and positive feedback over the iron electrodes, which are observed as two sharp plateaus with size (FWMH ≈ 1050 μm) and position in good correspondence with the two cathodes. Representative line scans recorded with the tip biased at +0.40 V for the oxidation of the mediator along an arbitrary line across the sample are presented in Figure 7 (a) using the raw current values. Apart from the variation in the base line, the shape of the feedback profiles is quite stable (the current increase after 24 hours resulted from electrochemical cleaning of the tip). The current profile measured over the remote cathode is uniform and shows a flat electrode with a clean surface, while the inner cathode reveals local minima which are reproducible between scans. The signal for the zinc anode is residual, which is not surprising given the small size of the electrode, as well as its recession due to dissolution.

Amperommetric sensing of dissolved oxygen revealed the depletion sites by a drop of the reduction current to values close to zero with the probe biased at -0.50 V; a significant and uniform depletion of oxygen was observed at the remote cathode, while on inner cathode the depletion was also observed, though less uniform - Figure 7 (b). On the zinc electrode there was no sign of depletion, mostly because the local alkalinisation at the tip determined by the cathodic reaction is likely to cause precipitation of zinc products on the platinum and consequent blocking of the tip.
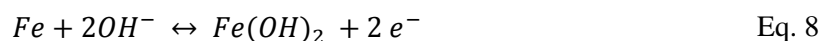
3.4 Ionic currents and pH distribution

The ionic current and the pH distribution measured by the SVET and the SIET probes are depicted in Figure 8. The SVET reveals a single anode, corresponding to zinc cations diffusing from the source of positive current flow, whereas the shape and size of the cathodes are in good agreement with the position of the iron plates and the current corresponds to an upward flow of OH⁻ anions, i.e. negative current. Despite the noise associated with the measurements, the two cathodes are well resolved, i.e., the two cathodes are separated by a region of nearly zero current, corresponding to the resin. The currents gradually decreased with time, but we could not identify the corrosion products or detect any local inhibition of cathodic reaction on iron from observation of the ionic current profiles.

The bulk pH measured with the microelectrode was ~5.5, in agreement with the measurement performed with the pH meter before starting the experiment. On zinc there was no sign of acidification that could result from local hydrolysis, whereas a strong alkalinisation on the cathodes was detected, with the pH reaching up to 10.5; a slight difference was observed between the two cathodes, with a slightly lower pH at the inner cathode. Further, the insulating region between the two cathodes also reached a high pH as a result of the flow of hydroxyl ions from the remote cathode. Naturally, these values are measured at some distance from the surface, and even higher values on the surface can be expected; a point measurement made with the tip of the pH probe touching the iron, pH 11 was recorded which is roughly 0.5 pH units higher than the value measured during the scan at a distance of 50 μm from the surface.

4. Discussion

The cathodic reaction caused a very strong alkalinisation from bulk pH 5.5 to pH 10.5 and reaching 11 at the very surface of the iron. In naturally aerated aqueous solutions of this pH, iron spontaneously becomes passive when corroding freely. If taking Fe(OH)$_2$ as passivating speciesthe reversible potential (for Eq. 8) at pH 11 is -0.941V [36], which is above the measured mixed potential of the system.

$$Fe + 2OH^- \leftrightarrow Fe(OH)_2 + 2\,e^- \qquad\qquad \text{Eq. 8}$$

This means that, at the spontaneous corroding potential measured for the galvanic model, iron is cathodically polarized into its region of thermodynamic immunity, with a conductive surface exposed and available for the reduction of oxygen.

While the primary cathodic reaction is the reduction of oxygen occurring under diffusion control, the potential for the reduction of water at pH 11 is -0.894 V (vs. SCE) and therefore the reduction of water can also occur as a secondary reaction.

Meanwhile, the solubility of zinc ions at pH 5.5 is very high [40], as given by the equilibrium concentration for Zn^{2+} with $Zn(OH)_2$:

$$\log(Zn^{2+}) = 12.26 - 2pH \qquad \text{Eq. 9}$$

This means that zinc ions cannot precipitate on zinc, but instead diffuse along the surface and migrate towards the cathodes [7, 8, 31]. Hydroxyl ions resulting from the cathodic reaction counter-diffuse in the direction of the anode. The diffusion of OH^- is confirmed by the alkalinisation of the electrolyte between the two cathodes and corresponding to a resin region, where the pH is quite high, reaching ~10. The hydroxyl ions never reach the anode because they react with the zinc cations, either forming $Zn(OH)^+$ or precipitating as $Zn(OH)_2$.

The precipitation sites are not at the edge of the cathode, but rather at a distance of ~ 150 μm. This location of the corrosion products is remarkably similar to that of a cut edge [28] despite the different geometry. Precipitation is dictated by the pH and zinc cation concentration. Figure 9 shows the stability diagram of different zinc species in 10 mM chloride and 5microM carbonate solution, calculated using Hydra-Medusa® software [39] and assuming the concentration of zinc in solution is 10^{-5} M [24]. The remaining constants used for calculation were as provided by the software database. For pH < 9.0 the conditions are not favourable for precipitation of zinc corrosion products, whereas for higher pH, $Zn(OH)_2$ and ZnO become stable. This prediction is consistent with the visual aspect of the surface during the pH mapping with the SIET. The reaction of zinc hydrolysis has a buffering effect and is consistent with the maintenance of pH values below ~ 9.0 in the vicinity of the zinc and at edge of the inner iron cathode, favouring the stability of zinc soluble species ($ZnOH^+$), whereas closer to the center of the plate the pH is sufficiently high for formation $Zn(OH)_2$ and ZnO[31].

A rough geometrical correlation between the corrosion products and the ionic current measurements was observed in previous work in which cut edge electrodes were used, i.e., with no gap between anode and cathode [28, 41]. This discrepancy may be explained by the cancellation of positive and negative currents in the measurement when the electrodes are in very close proximity, i.e., by attenuation of the concentration gradients in a microscopic narrow region in the vicinity of the probe [42]. Therefore, we conclude that the local ionic currents do not reveal any self-healing effect. Other authors, like, Krieg et al [12], Mouanga [17, 18] and Ogle in recent works [14,15, 16] suggest that corrosion products may not cause cathodic inhibition by themselves, but rather participate in synergistic effect between zinc cations and the

native iron oxides on the iron surface. However, we find no proof of iron passivity and we propose that the corrosion products formed, most likely $Zn(OH)_2$ and ZnO are not adherent and are dragged by moving probe stirring the solution, thus explaining the cathodic activity.

Globally, we observed that all the techniques provided valuable information about the model system. Naturally, the duration as well as the ease of setting up an experiment was quite different. Most importantly, the tip-to-sample distance and the scan rate have an influence on the ability of microprobe techniques to measure cathodic inhibition. The SECM is not a straightforward technique as the Pt-electrodes can easily become contaminated from species in solution and local alkalinisation while scanning at cathodic potentials may introduce some artefacts in the results. However, the small distance of the tip to the working electrode and the slow scan rate made it the most sensitive to the geometry and morphology of the surface of the model. The zinc anode gave only a minor signal in the feedback mode possibly due to a small efficiency of the metal to the regeneration of the mediator but mostly because of recession of the dissolving surface during the experiment, bringing the diffusion layer away from the probe. The technique gave a distinct pattern on the "clean" cathode (Fe2) and on the cathode covered with corrosion products (Fe1), on which the regeneration current has consistent local minima. These minima can be explained by the precipitation of corrosion products which create topographic features that reduce the volume of electrolyte under the microprobe and cause a local minimum of the feedback current. Further, a slight increase in the tip current operating in the redox competition mode while scanning the inner iron surface, suggests a minor barrier effect on the cathodic reaction due to the presence of those products.

The LEIS has a comparatively low resolution, due to the large separation of the bi-probe Pt-wires and a high probe-to-sample distance (> 100 μm). It was found to be quite sensitive to the zinc anode, but a significant difference in the behaviour of each cathode surface was observed on the constant frequency scan at 1Hz. For shorter exposure times, the inner cathode did not produce a response to the excitation signal. Since the electrodes behave as a constant phase element at 1 Hz, a small perturbation in the sample potential should produce fluctuations in the double layer, i.e., on the charged particles at the sample/electrolyte interface which control the passage of ionic currents into bulk solution. The explanation for absence of a.c. current takes into account the reactions occurring above the inner cathode, in bulk solution, i.e. closer to the tip. These reactions, which occur at a high rate, are chemical in nature, and thus do not respond to the small a.c. stimulus applied to the system, thus decreasing the a.c. current below the noise level. At a later stage of the corrosion processes, once a pseudo-steady state is achieved, a higher concentration of free ions is reached over the inner cathode, with a consequent increase of conductivity of the electrolyte and thus an apparent increase of the admittance. Further, any variation in the capacitive response of the inner cathode due to the

formation of a dielectric layer of zinc oxide would go easily undetected in impedance measurements as this dielectric layer is coupled in parallel with the double layer capacitance (10^{-4} Fcm^{-2}s^{n-1}, n=0.85) of the bare iron interface.

In summary, as a result of the probe height and of the probe size, the SECM gives the best identification of the size and location of the cathodes, particularly in the feedback mode, but it is not adequate for the narrow zinc anode, which in turn was well identified and monitored by the SVET and the LEIS. The residual a.c. admittance in the inner cathode in the initial stages of exposure provides an insight into the nature of the reactions occurring at different regions of the cathode. Except for the SVET, all localized techniques allowed observation of modifications on the electrochemical reactivity of the iron surface due to the presence of zinc corrosion products. For these conditions of pH and anode-to-cathode ratio, a self-healing effect caused by the precipitation of zinc corrosion products could not be observed, although a minor barrier effect of the poorly adherent oxides may be detected under conditions of little mechanical interaction of the probe with the substrate.

5. Conclusions

The use of an asymmetric three-electrode model system consisting of a thin zinc anode foil and two iron plate cathodes was beneficial for the understanding of the galvanic corrosion of Fe-Zn cut edge systems in the microscopic scale, as it minimizes the direct interference of each electrode on the local electrochemical responses; further, it evidenced the diffusion processes occurring above the cathode, namely the diffusion of hydroxyl ion towards the anode.

The cathodic reactions, mainly oxygen reduction, occur on an immune iron surface. The SVET revealed a reasonably uniform distribution of the cathodic reaction along the iron surface, despite the abundant precipitation of corrosion products on the region closer to the anode, i.e., there were no signs of cathodic inhibition caused by the zinc corrosion products. Meanwhile, the overall current density measured across the sample decreased with time as the system became less active and tended to nearly steady-state. The precipitation of zinc oxide occurs at some distance from the cathode edge, beyond a narrow region where precipitation was not registered. The absence of precipitation in this region results not from suppression of cathodic activity but rather from the counter-diffusion of Zn^{2+} and of OH^- ions that determines the point at which the critical pH for precipitation of zinc corrosion products is reached.

The local current generated by the anode was not sensed using the SECM tip, whereas the LEIS and the SVET have proved greater sensitivity to the zinc. Further, the zinc corrosion products were detected by the SECM, in the form of reproducible minima in the feedback current. The LEIS technique was found to be unable to measure cathodic activity on

the cathode covered by zinc corrosion products in the early stages of immersion whereas results for longer immersion times reflect an increase in the solution conductivity.

References

1. A. P. Yadav, H. Katayama, K. Noda, H. Masuda, A. Nishikata, T. Tsuru, Potential distribution over a zinc/steel galvanic couple corroding under thin layer of electrolyte, Electrochem. Acta 52 (2007) 3121-3129
2. S. Thomas, N. Birbilis, M. S. Venkatraman, I. S. Cole, Corrosion of zinc as a function of pH, Corrosion 68 (2013) 015009-1-9
3. K. Ogle, V. Baudu, L. Garrugues, X. Philippe, Localized electrochemical methods applied to cut edge corrosion, J. Electrochem. Soc. 147 (2000) 3654-3660
4. F. Thébault, B. Vuillemin, R. Oltra, K. Ogle, C. Allely, Investigation of self-healing mechanis on galvanized steels cut edges by coupling SVET and numerical modeling, Electrochim. Acta 53 (2008) 5226-5234
5. F. Thébault, B. Vuillemin, R. Oltra, C. Allely, K. Ogle, Protective mechanisms occurring on zinc coated steel cut-edges in immersion conditions, Electrochim. Acta 56 (2011) 8347-8357
6. E. Tada, K. Sugawara, H. Kaneko, Distribution of pH during galvanic corrosion of a Zn/steel couple, Electrochim. Acta 49 (2004) 1019-1026
7. E. Tada, S. Satoh, H. Kaneko, The spatial distribution of Zn^{2+} during galvanic corrosion of a Zn/steel couple, Electrochim. Acta (2004) 2279-2285
8. E. Tada, H. Kaneko, Optical visualization of concentration field of Zn^{2+} during galvanic corrosion of a Zn/steel couple, Corr. Sci. 52 (2010) 3421-3427
9. S. Bonk, M. Wicinski, A. W. Hassel, M. Stratmann, Electrochemical characterizations of precipitates fromed on zinc in alkaline sulphate solution with increasing pH values, Electrochem. Comm. 6 (2004) 800-804
10. V. Ligier M. Wéry, J.-Yves Hihn, J. Faucheu, M. Tachez, Formation of the main atmospheric zinc end products: $NaZn_4Cl(OH)_6SO_4 \cdot 6H_2O$, $Zn_4SO_4(OH)_6 \cdot nH_2O$ and $Zn_4Cl_2(OH)_4SO_4 \cdot 5H_2O$ in [Cl⁻][SO_4^{2-}][HCO_3^-][H$_2$O$_2$]electrolytes, Corr. Sci. 41 (1999) 1139-1164
11. V. Padilla, A. Alfantazi, Corrosion film breakdown of galvanized steel in sulphate-chloride solutions, Construction and Building Materials 66 (2014) 447-457
12. R. Krieg, M. Rohwerder, S. Evers, B. Schuhmacher, J. Schauer-Pass, Cathodic self-healing at cut-edges: The effect of Zn^{2+} and Mg^{2+} ions, Corr. Sci. 65 (2012) 119-127
13. H. Tanaka, J. Wakatsuki, K. Kandori, T. Ishikawa, T. Nakayama, Role of zinc compounds on the formation, morphology, and adsorption characteristics of $\beta - FeOOH$ rusts, Corr. Sci. 52 (2010) 2973-2978

14. J. D. Yoo, P. Volovitch, A. Adbel Aal, C. Allely, K. Ogle, The effect of an artificially synthesized simonkolleite layer on the corrosion of electrogalvanized steel, Corr. Sci. 70 (2013) 1-10

15. J. D. Yoo, K. Ogle, P. Volovitch, The effect of synthetic zinc corrosion products on corrosion of electrogalvanized steel: I. Cathodic reactivity under zinc corrosion products, Corr. Sci. 81 (2014) 11-20

16. J. D. Yoo, K. Ogle, P. Volovitch, The effect of synthetic zinc corrosion products on corrosion of electrogalvanized steel: II. Zinc reactivity and galvanic coupling zinc/steel in presence of zinc corrosion products, Corr. Sci. 83 (2014) 32-37

17. M. Mouanga, P .Berçot, J. Y. Rauch, Comparision of corrosion behavior of zinc in NaCl and in NaOH solutions. Part I. Corrosion layer characterization, Corr. Sci. 52 (2010) 3984-3992

18. M. Mouanga, P .Berçot, Comparision of corrosion behavior of zinc in NaCl and in NaOH solutions. Part II. Electrochemical analyses, Corr. Sci. 52 (2010) 3993-4000

19. H.S. Isaacs, Y. Ishikawa, Applications of the vibrating probe to localized current measurements, in: R. Baboian (Ed.), Electrochemical Techniques for Corrosion Engineering, NACE, Houston, TX (1986), pp. 17-23

20. Worsley, H.N. McMurray, A. Belghazi, Determination of localized corrosion mechanisms using a scanning vibrating reference electrode technique, Chem. Commun. (1997) 2369-2370

21. F. Zou, C. Barreau, R. Hellouin, D. Quantin, D. Thierry, Application of scanning vibrating electrode techniques to study the degradation of coil-coated steel at edges, Mater. Sci. Forum, 289-292 (1998) 83-92

22. B. M. Fernández-Pérez, J. Izquierdo, S. González, R. M. Souto, Scanning electrochemical microscopy studies for the characterization of localized corrosion reactions at cut edges of coil-coated steel, J. Solid. State Electrochem. 18 (2014) 2983-2992

23. J. Izquierdo, L. Nagy, A. Varga, J. J. Santana, G.Nagy, R. M. Souto, Spatially resolved measurement of electrochemical activity and pH distributions in corrosion processes by scanning electrochemical microscopy using antimony microelectrode tips, Electrochim. Acta 56 (2011) 8846-8850

24. R. M. Souto, Y. G. Garcia, D. Battistel, S. Daniele, On the use of mercury coated tips in scanning electrochemical microscopy to investigate galvanic corrosion process involving zinc and iron, Corr. Sci. 55 (2012) 401-406

25. A. Alvarez-Pampliega, S.V. Lamaka, M.G. Taryba, M. Madari, J. De Strycker, E. Tourwé, M.G.S. Ferreira, H. Terryn, Cut-edge corrosion study on painted aluminum rich metallic coated steel by scanning vibrating electrode and micro-potentiometric techniques, Electrochim. Acta, 61 (2012) 107-117

26. A.C. Bastos, A.M. Simões, M.G. Ferreira, Corrosion of electrogalvanized steel in 0.1 M NaCl studied by SVET, Port. Electrochim. Acta, 21 (2003) 371-387

27. A.M. Simões, A.C. Bastos, M.G. Ferreira, Y. González-García, S. González, R.M. Souto, Use of SVET and SECM to study the galvanic corrosion of an iron-zinc cell, Corros. Sci., 49 (2007) 726-739

28. A.G. Marques, J. Izquierdo, R.M. Souto, A.M. Simões, SECM imaging of the cut edge corrosion of galvanized steel as a function of pH, Electrochim. Acta (2015) 238-245

29. M. Mouanga, M .Puiggali, B Tribollet, V. Vivier, N. Pébère, O. Devos, Galvanic corrosion between zinc and carbon steel investigates by local electrochemical impedance spectroscopy, Electrochim. Acta 88 (2013) 6-14

30. F. Thébault, B. Vuillemin, R. Oltra, C. Allely, K. Ogle, Modeling bimetallic corrosion under thin electrolyte films, Corr. Sci. 53 (2011) 201-207

31. V. Topa, A.S. Demeter, L. Hotoiu, D. Deconinck, J. Deconinck, A transient multi-ion transport model for galvanized steel corrosion protection, Electrochim. Acta 77 (2012) 339-347

32. A. J. Bard, F-R. F. Fan, J. Kwak, O. Lev, Scanning electrochemical microscopy: introduction and principles, Anal. Chem., 61 (1989) 132-138

33. D. O. Wipf, A. J. Bard, Scanning electrochemical microscopy. VII. Effect of heterogeneous electron-transfer rate at the substrate on the tip feedback current, J. Electrochem. Soc. 138 (1991) 469-474

34. S. V. Lamaka, M. Taryba, M. F. Montemor, H. S. Isaacs, M. G. S. Ferreira, Quasi-Simultaneous Measurements of ionic currents by vibrating probe and pH distribution by ion-selective microelectrode, Electrohem. Comm. 13 (2011) 20-23

35. R. D. Perry, C.H. Chilton, Chemical Engineer's Handbook, 5th Edition, International Student Edition, McGraw-Hill (1974), Tokyo, Japan

36. M. Pourbaix, Atlas of Electrochemical Equilibra in Aqueous Solutions, National Association of Corrosion Engineers, Houston, Texas, 1974

37. A. Nazarov, D. Thierry, Rate-determining reactions of atmospheric corrosion, Electrochim. Acta 49 (2004) 2717-2724

38. A. Cachet, R. Wiart, The kinetics of zinc dissolution in chloride electrolytes: Impedance measurements and electrode morphology, J. Electroanal. Chem. 111 (1980) 235–246

39. Software available at: <https://www.kth.se/en/che/medusa/chemeq-1.369367>, 2015.

40. D. D. Perrin, International Union of Pure and Applied Chemistry. Commision on Electroanalytical Chemistry, Dissociation constants of inorganic acids and bases in aqueous solution, Butterworths, London, 1969

41. A.M. Simões, J. Torres, R. Picciochi, J.C.S. Fernandes, Corrosion inhibition at galvanized steel cut edges by phosphate pigments, Electrochim. Acta, 54 (2009) 3857-3865

42. A.C. Bastos, M. C. Quevedo, M. G. S. Ferreira, The influence of vibration and probe movement on SVET measurements, Corr. Sci. 92 (2015) 309-314